Doctoral School of Clinical Medicine

Albert Szent-Györgyi Medical School

University of Szeged

Defining the True Extent of Glioblastoma Based on Probabilistic Tractography and FLAIR Images

Ph.D. Dissertation

Bayan Shukir

Supervisor: Prof. Dr. Pál Bárzo, MD, Ph.D., MSc

Co-Supervisor: Asst. Prof. Dr. David Kis, MD, Ph.D.

Szeged 2025

Publications directly related to the subject of the thesis:

I. David Kis, Laszlo Szivos, Mark Rekecki, Bayan Shukir, Adrienn Mate, Katalin Hideghety and Pal Barzo. 2022. Predicting the True Extent of Glioblastoma Based on Probabilistic Tractography. Front. Neurosci. 16:886465. https://doi.org/10.3389/fnins.2022.886465. **IF: 4.3**

II. Bayan Shukir, Laszlo Szivos, Pal Barzo, and David Kis. 2025. Preoperative FLAIR Images for Identifying Glioblastoma Boundaries. BMC Medical Imaging 25:302. https://doi.org/10.1186/s12880-025-01839-2. **IF: 3.2**

Table of Contents

Summary

Glioblastoma is the most aggressive and fast-growing tumor of the central nervous system. Surgery provides the best survival rate for patients with this tumor. However, the recurrence is almost inevitable, as microscopic tumor cells infiltrate surrounding tissues. Therefore, accurately identifying the true extent of glioblastoma is crucial for improving survival outcomes and minimizing the risk of severe, permanent neurological deficits associated with surgery.

In this Ph.D. thesis, we provide new insights into this critical aspect by evaluating the reliability of two distinct approaches: 1, probabilistic tractography and 2, preoperative FLAIR imaging. To the best of our knowledge, no previous studies have examined these approaches before.

Probabilistic tractography is an advanced imaging method that can potentially be used to identify infiltrated pathways. It tracks fibers in regions with low anisotropy values and visualizes crossing fibers. Moreover, it provides quantitative measures representing the connectivity distribution of the seed region. In this study, we examined the sensitivity and specificity of probabilistic tractography at different threshold levels to determine which one provide the highest probability of the true extent of the tumor. On the other hand, fluid-attenuated inversion recovery (FLAIR) imaging is believed to be the most sensitive conventional MRI modality for detecting infiltrated tumor cells. Our study investigated the sensitivity and specificity of preoperative FLAIR imaging to delineate the true boundaries of glioblastoma.

The results of the two studies suggests that while FLAIR is effective as a radiologic imaging tool, its prognostic value is limited. Probabilistic tractography on the other hand, emerges as a more reliable method for predicting the true extent of glioblastoma at the time of diagnosis, with high sensitivity and specificity.

1. Introduction

Glioblastoma is the most aggressive and frequent type of primary central nervous system tumors (CNS), classified as grade 4 according to the world health organization (WHO) classification system. This classification is based on histological malignancy, mitotic activity and molecular genetic markers, distinguishing gliomas into low-grade (1-2) and high-grade (3-4) categories (Louis et al., 2021).

Unfortunately, all the advanced therapies are less effective. Most of the patients die within 16–20 months after the diagnosis (Yan et al., 2009). The therapeutic protocol is maximal safe resection (more than 90% of the tumor mass should be removed) and the Stupp protocol onwards (Stupp et al., 2005; Louis et al., 2021; Ostrom et al., 2021).

Glioblastoma is an aggressive and infiltrative malignant tumor which originates from the glial cells of the white matter. During the tumor progression the glioblastoma cells are propagating along fiber tracts. In the advanced stage, the tumor can will infiltrate gray matter also (Wirsching et al., 2016).

The most widely used radiological modality for glioblastoma diagnosis is the contrast-enhanced T1 magnetic resonance imaging (CE-T1 MRI). The tumor has a very typical characteristic on the MR images as it commonly looks like an irregular ring-shaped contrast enhancement with a hypointense necrotic center, usually surrounded by prominent peritumoral edema and mass effect (Young, 2007; Shukla et al., 2017). We know it from previous studies that the tumor mass on the MRI images does not correspond to the real extent of the tumor (Demuth and Berens, 2004). Because of the glioblastoma's infiltrative growth, tumor cells can be present far away (5 to 10 cm) from the contrast-enhancing border. Other studies have demonstrated that glioblastoma cells are present in the whole brain (Tonn and Goldbrunner, 2003).

Tumor cells are spreading along fiber tracts infiltrating brain regions far away from the original site of the tumor. The true extent of the glioblastoma consists the tumor mass and infiltrative part also only the tumor mass can be visualized accurately on the standard MRI images (Petrecca et al., 2013; Lemee et al., 2015). The infiltrative component is basically an abnormal "fiber tract" which invades and destroys normal white matter pathways (Virga et al., 2019). The recurrence of glioblastoma usually originates from these this part, which is supported by the observation that tumor progression often appears in the white matter surrounding the resection cavity (Milano et al., 2010; Petrecca et al., 2013).

Because of this aggressive and infiltrative feature of glioblastoma, effective treatment is challenging. The surgical goal is to resect the tumor which is visible on the MRI images. The remaining tumor cells usually represents a significant volume even if the post-operative MRI shows a gross total resection. These are treated with irradiation and chemotherapy (Stupp et al., 2005). The patients' survival depends on how the remaining tumor cells respond to these oncological treatments. The effectiveness of these treatments are higher if the residual tumor volume is lower (Roelz et al., 2016).

As opposed to chemotherapy, which is a systematic treatment, surgery and irradiation are focal treatments and can be individually tailored to achieve the best results. Surgery is considered successful if no more than 1 cc residual contrast enhancement is visible on the post-operative MRI images. Irradiation is typically focused to an area that exceeds the border of the resection cavity by 1 to 3 cm to destroy the infiltrative glioblastoma cells (Barani and Larson, 2015).

The patients' survival is defined by several factors, such as age, comorbidities, extent of resection, location of tumor, Karnofesky Performance Scale and molecular markers (e.g., MGMT promoter methylation, IDH mutant or wild type) (Lacroix et al., 2001; Bauchet et al., 2010). Theoretically, longer survival could be accomplished if the residual tumor volume could be minimized. One way to do so is the so called "supratotal" tumor resection (when the resection margins exceed the contrast-enhancing border) or individually planned irradiation that focuses to brain regions actually really infiltrated by the tumor (De Bonis et al., 2013). Unfortunately, to date, standard MRI sequences cannot identify infiltrated brain regions reliably (Shukla et al., 2017; de Leeuw and Vogelbaum, 2019). Recent studies have shown that gross total resection is an independent prognostic factor associated with improved clinical outcomes (Wykes et al., 2021).

In the last decade, FLAIR imaging has become essential in glioblastoma assessment. Due to the infiltrative nature of the glioblastoma the postcontrast enhancement alone is insufficient in the definition of the radiological feature of the tumor (Wen et al., 2010). FLAIR images have an increased sensitivity in detecting microscopic tumor infiltration and noncontrast enhancing lesions (Cha, 2009). Hyperintensity on FLAIR imaging often extends beyond the contrast-enhancing part of a glioblastoma tumor. Due to that, recently an increased interest is focused into the FLAIR changes around the tumorous area (Aydin et al., 2001; Brandes et al., 2009; Rapp et al., 2017). The hyperintense region observed on the FLAIR images believed to correspond to both microscopic tumor cells and edema (Verburg et al., 2020). Other studies demonstrated that FLAIR signal abnormalities

represent infiltrative tumor cells and the survival rate correlates with the amount of this abnormality around the tumor (Haddad et al., 2022). More than 90% of tumor recurrences will occur within this FLAIR hyperintense regions (Petrecca et al., 2013). These properties of FLAIR play a images can play an important role in the diagnosis of tumor progression and recurrence (Winterstein et al., 2010; Sarbu et al., 2016; Quan et al., 2018). Several studies have tried to correlate patient outcome to the maximal safe resection of both the contrast-enhancing and FLAIR hyperinmtense tumor but the results are controversial. Some studies have shown that including the FLAIR hyperintense regions into the resection is associated with better outcome (Li et al., 2016; Certo et al., 2019; de Leeuw and Vogelbaum, 2019). On the other hand, some studies did not find any correlation between the extent of FLAIR signal abnormality and the survival (Altieri et al., 2019). Despite the potential benefit of FLAIR imaging to visualize the true extent of glioblastoma, increase the effectiveness of surgical resection and radiation therapy, its prognostic value remains unclear (Woodroffe et al., 2020).

The majority of studies have been investigated the connection between the FLAIR abnormalities as a potential indicator of survival in glioblastoma patients. To the best of our knowledge, no previous study has ever assessed to verify the sensitivity and specificity of the preoperative FLAIR images to define the true extent of the glioblastoma.

Tractography is an advanced application of diffusion MRI. Based on the diffusion movement pattern of the water molecules, white matter fiber tracts can be visualized (Le Bihan et al., 1992; Mascalchi et al., 2005). The diffusion pattern is characterized by anisotropy: if the diffusion is more directional the anisotropy becomes higher and fiber tract reconstruction is more certain in these brain regions. Tractography has become a popular tool in preoperative brain mapping and image guided therapy in brain tumor patients (Costabile et al., 2019). There are two types of tractography, the deterministic and probabilistic methods (Yamada et al., 2009).

Conventional diffusion tensor imaging-based deterministic tractography can visualize the major white matter pathways reliably (Mori and van Zijl, 2002; Mukherjee et al., 2008) Therefore, it can be used to and identify white matter fibers pathways around the tumor (e.g., corticospinal tract) and help to plan the surgical trajectory to avoid injuring important pathways. The main limitation of deterministic tractography is that in regions with low anisotropy (cortical and subcortical gray matter, branching pathways, crossing fibers), it cannot identify the fibers reliably (Yamada et al., 2009).

The ball and sticks model-based probabilistic tractography has several advantages and overcomes the above limitation. It can identify fibers in low anisotropy regions and provides quantitative measures representing the connectivity pattern of the brain region. It can be thresholded to exclude false positive results (Behrens et al., 2003b, 2007). Probabilistic tractography is a potential tool to identify the infiltrated fiber tracts in glioblastoma patients (Behrens et al., 2007; Kis et al., 2014).

2. Objectives

The aim of the two projects was determining the true extent of glioblastoma on advanced MRI modalities, as the standard imaging methods are not capable of visualizing the infiltrated brain tissue. This could initiate individual surgical and irradiation treatment and result in longer survival and better quality of life.

The first study, "Predicting the True Extent of Glioblastoma Based on Probabilistic Tractography," utilizes diffusion tensor imaging (DTI) and probabilistic tractography to estimate tumor spread along white matter tracts. The second study, "Preoperative FLAIR Images for Identifying Glioblastoma Boundaries," investigates the diagnostic value of FLAIR hyperintensity as non-invasive indicator of the infiltrative tumor margins. By assessing the sensitivity and specificity of both methods, these studies sought to establish a clinically reliable and applicable imaging protocol for pretreatment planning.

3. Materials and methods

3.1 Study design

The methodology of both studies followed the same protocol as it is described in details below. There were minor adjustments in patient population, and data processing techniques in the FLAIR study group.

3.2 Patient population

Patients were selected retrospectively from individuals whom underwent surgical treatment at the Neurosurgery Department between 2010 and 2021. The inclusion and exclusion criteria were as follows: 1, The diagnosis was high grade glioma (primary glioblastoma or grade 3 anaplastic oligodendroglioma). 2, All patients underwent either subtotal or total tumor resection during the primary surgery (according to post-operative MR images acquired within 48 h). Subtotal resection was defined as the remaining contrast enhancing tumor was less than 10% of its original volume, while greater extent of remaining tumor is considered as partial resection. Total resection was achieved when no contrast enhancement was visible (Ahmed et al., 2019). The surgical resection was followed by the Stupp protocol (Stupp et al., 2005). 3, All patients had preoperative DTI and FLAIR scans in addition to the routine head MRI protocol. 4, Follow-up MRI scans were acquired every 3 months. A total of 96 adult (>18 years) patients were screened and 20 were enrolled to the probabilistic tractography study and 16 were included in the FLAIR study. Both studies shared the same exclusion criteria, which was 1, loss to follow-up or 2, partial surgical resection.

Follow-up MRI was utilized to identify infiltrated fiber tracts that had prominent tumor recurrence in the surrounding white matter. The tumor recurrence was considered to be the newly appeared contrast enhancement around/in the resection cavity.

Ethical approval was received from the Institutional Review Board (IRB) of the Medical Faculty, University of Szeged. The requirement for informed consent was obtained from all patients.

Patients' clinical data are summarized in Table 1, Appendix 1.

3.3 Imaging techniques

Preoperative and follow-up MR images have been utilized in both studies. Scanning was performed using a 3T GE Signa Excite scanner. Preoperative MRI sequences which were used in the studies are the following (1) contrast-enhanced high-resolution 3D

axial FSPGR-T1 (CE-T1); (2) diffusion-weighted image (DTI) and (3) fluid attenuation inversion recovery (FLAIR) images. For the follow-up MRI, only the contrast-enhanced high resolution 3D axial FSPGR-T1 sequence was used.

Contrast-enhanced high-resolution T1-weighted scan parameters: 3D FSPGR fast spoiled gradient echo: repetition time [TR]/echo time [TE], 10.3/4.2 ms; flip angle, 15; ASSET 2; field of view [FOV] 25 cm x 25 cm; matrix, 256 x 256; slice thickness, 1 mm (voxel dimension was 1x1x1 mm^3).

Diffusion-weighted image parameters: DTI: TR/TE, 11,500/98.4 ms; flip angle, 90; FOV, 24 cm x 24 cm; matrix, 80 x 80; slice thickness, 3 mm; ASSET: 2; b-value = 1,000 s/mm2, in 25 independent directions and 1 non-gradient set (b-value = 0 s/mm2) (voxel dimension was 3x3x3 mm^3)

FLAIR scanning parameters: 3D CUBE; TR/TE, 6,000/140 ms; FOV, 25 × 25 cm; slice thickness 1 mm; and matrix, 256 × 256 (voxel dimension was 1x1x1 mm^3).

Scans covered the whole head. Total scan time was 18–27 min, including the following sequences (FLAIR, non-contrast and contrast-enhanced T1, T2, DWI, DTI, SWI).

3.4 Image processing and registration

According to the method previously described by Behrens et al. (2003a), MRI data were processed using tools from the FMRIB Software Library (FSL, version 5.0.7; Oxford Centre for Functional MRI of the Brain (FMRIB), United Kingdom) [11]. The original DICOM files were converted into compressed NifTI format using Chris Rordens' MRICron software (Rorden et al., 2007). FLAIR and diffusion images were visually checked for artifacts, and data quality was satisfactory across all subjects; therefore, no volume was discarded.

Standard preprocessing steps were applied to the DTI images. These included eddy current and motion correction (affine registration of the diffusion volumes to the b0 volume) and b-matrix adaptation using the eddy tool (FSL 6.0.1) (Andersson and Sotiropoulos, 2016) following the method of Leemans and Jones (2009). Skull stripping was performed, followed by reconstruction of diffusion tensors and estimation of diffusion parameters (Smith, 2002).

For each patient, DTI was registered to the preoperative CE-T1 weighted images using a 6 degrees of freedom transformation (cost function: mutual information, interpolation:

[1] www.fmrib.ox.ac.uk/fsl

trilinear). The same registration steps were applied for preoperative FLAIR images.

To do the analyses in the standard space, affine registration (12 degrees of freedom; cost function - correlation ratio, interpolation - trilinear) was performed to align each patient's preoperative CE-T1, FLAIR and follow-up CE-T1 images to the MNI152 1mm standard T1 brain template (Montreal Neurological Institute, MNI152 1 mm brain). Transformation matrices were generated at each registration step. All image registrations were conducted using FMRIB's Linear Image Registration Tool (FLIRT) (Jenkinson and Smith, 2001; Jenkinson et al., 2002).

3.5 Defining masks

Two types of masks were utilized: (1) tumor masks (primary tumor and tumor recurrence masks); and (2) cortical and subcortical white matter masks.

Tumor masks were employed to delineate the true extent of glioblastoma. In the probabilistic tractography study, the primary tumor mask served as the seed mask. In the FLAIR study, the primary tumor mask was defined by outlining the entire hyperintense region on the preoperative FLAIR images, reflecting both the solid part of the tumor and the infiltrating tumor cells along with the edema.

The tumor recurrence mask was used to identify brain regions which were initially infiltrated. Glioblastoma mostly recur in the 2-3 cm proximity of the border of the primary contrast-enhancing lesion. It is believed that the tumor cells were already present here but unable to detect on MRI yet. Therefore, the sites where the glioblastoma recurred correlates with the primarily infiltrated brain.

Cortical and subcortical white matter masks were applied to map regions of tumor infiltration as sites of recurrence, providing a detailed representation of affected brain areas.

3.5.1 Cortical and subcortical white matter masks

The standard brain was divided into distinct subcortical and cortical subregions. The standard Johns Hopkins University, international consortium of brain mapping, diffusion tensor imaging (JHU ICBM–DTI–white matter–81) labels map was used to segment the white matter into 54 subregions in the left and right hemispheres each, and 6 midline structures (Mori et al., 2008). The standard automated anatomical labeling atlas 3 (AAL3) map was used to segment the cortex into 84 subregions on each side (Rolls et al., 2020). The JHU–ICBM–DTI–white matter–81 labels and AAL3 maps were in the

MNI152 1 mm space (Hua et al., 2008; Rolls et al., 2020). Figure 1 A, B.

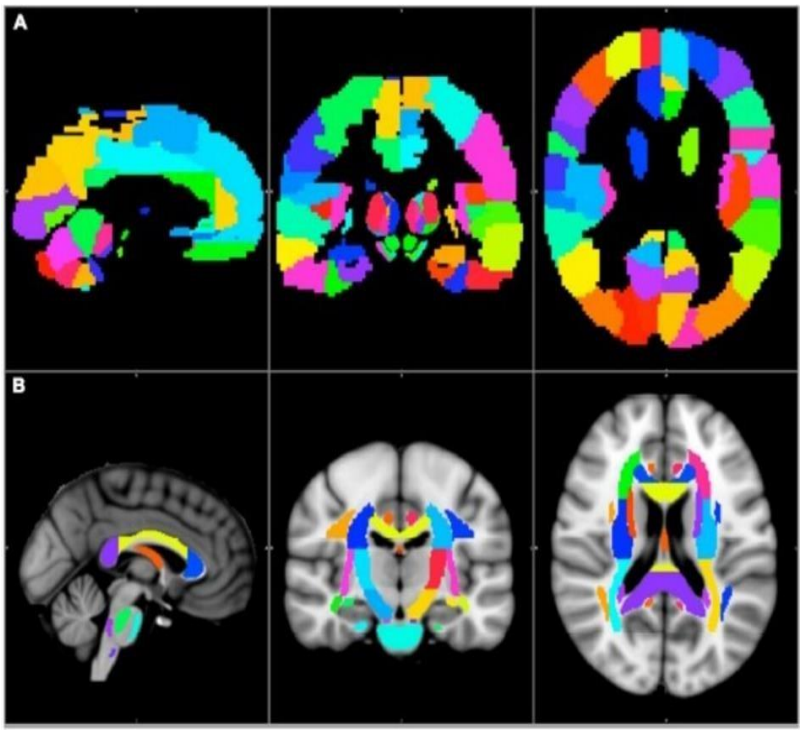

Figure 1: Brain regions in the MNI152 1-mm space. The (A) AAL3 cortical and (B) JHU–ICBM–DTI–81 white matter subcortical label.

3.5.2 Tumor masks

The primary tumor and the tumor recurrence masks were generated using patients' preoperative imaging data (CE-T1 and FLAIR images) and follow-up CE-T1-weighted images, respectively. The tumor observed on preoperative CE-T1 and FLAIR images was delineated based on two key features: the contrast-enhancing region on CE-T1 images and the hyperintense signal abnormalities observed on FLAIR images (the first was used in the probabilistic tractography study while the second one was applied in the FLAIR study. These features considered to represent the tumor's extent, encompassing both the enhancing core and infiltrative margins, (Figures 5 and 6).

For the probabilistic tractography study, the primary tumor mask served as the seed mask, enabling the identification of white matter pathways infiltrated by the tumor. Figures 2-4 provide a visual representation of these masks and their applications.

The tumor recurrence mask, identified on follow-up CE-T1 imaging, was considered the primary infiltrated brain region and served as the benchmark for the true extent of glioblastoma. The newly appeared contrast enhancement was considered as recurrence and delineated as the tumor recurrence mask.

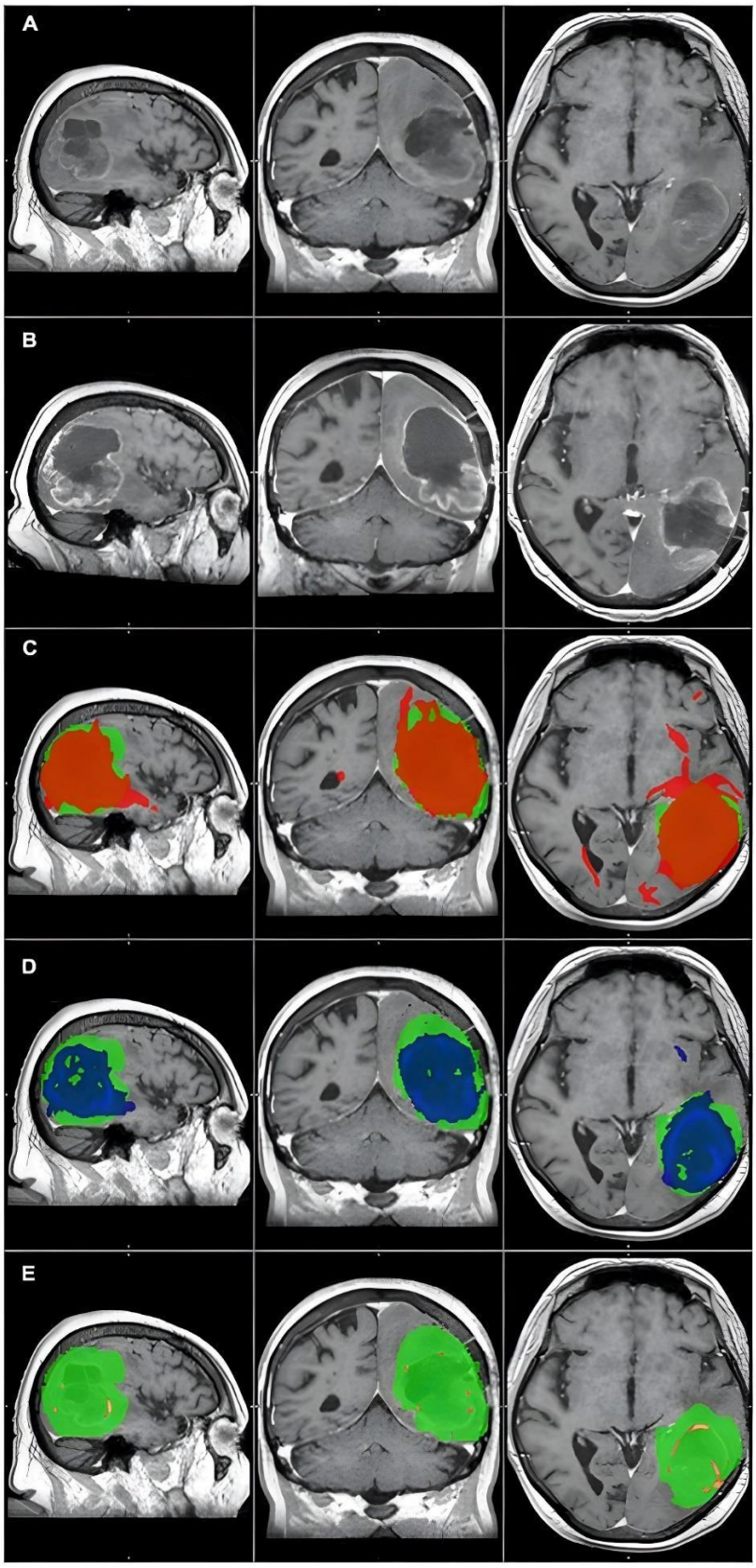

Figure 2: The primary tumor, the recurrence tumor, and the overlap between the different TCs and the tumor recurrence mask of the representative case of Patient 14 are displayed in this figure. All images are transformed to the MNI152 1 mm space. (A) The preoperative contrast enhanced T1 image. A huge tumor with ring shaped contrast enhancement can be seen in the left temporo-parito-occipital region. (B) The size and the location of the tumor recurrence. (C) The 1% TC (red) is overlapped on the tumor recurrence mask (green). (D) The 5% TC

(blue) is overlapped on the tumor recurrence mask (green). (E) The 40% TC (red-yellow) is overlapped on the tumor recurrence mask (green). (C–E) Are on the preoperative T1 images. Although the sensitivity is higher at 1% than at 5%, the specificity is lower due to the greater number of false positive regions. The best overlap can be seen at the 5% threshold level. At 40%, the TC is almost invisible and covers only a small portion of the tumor recurrence mask resulting in high specificity but low sensitivity.

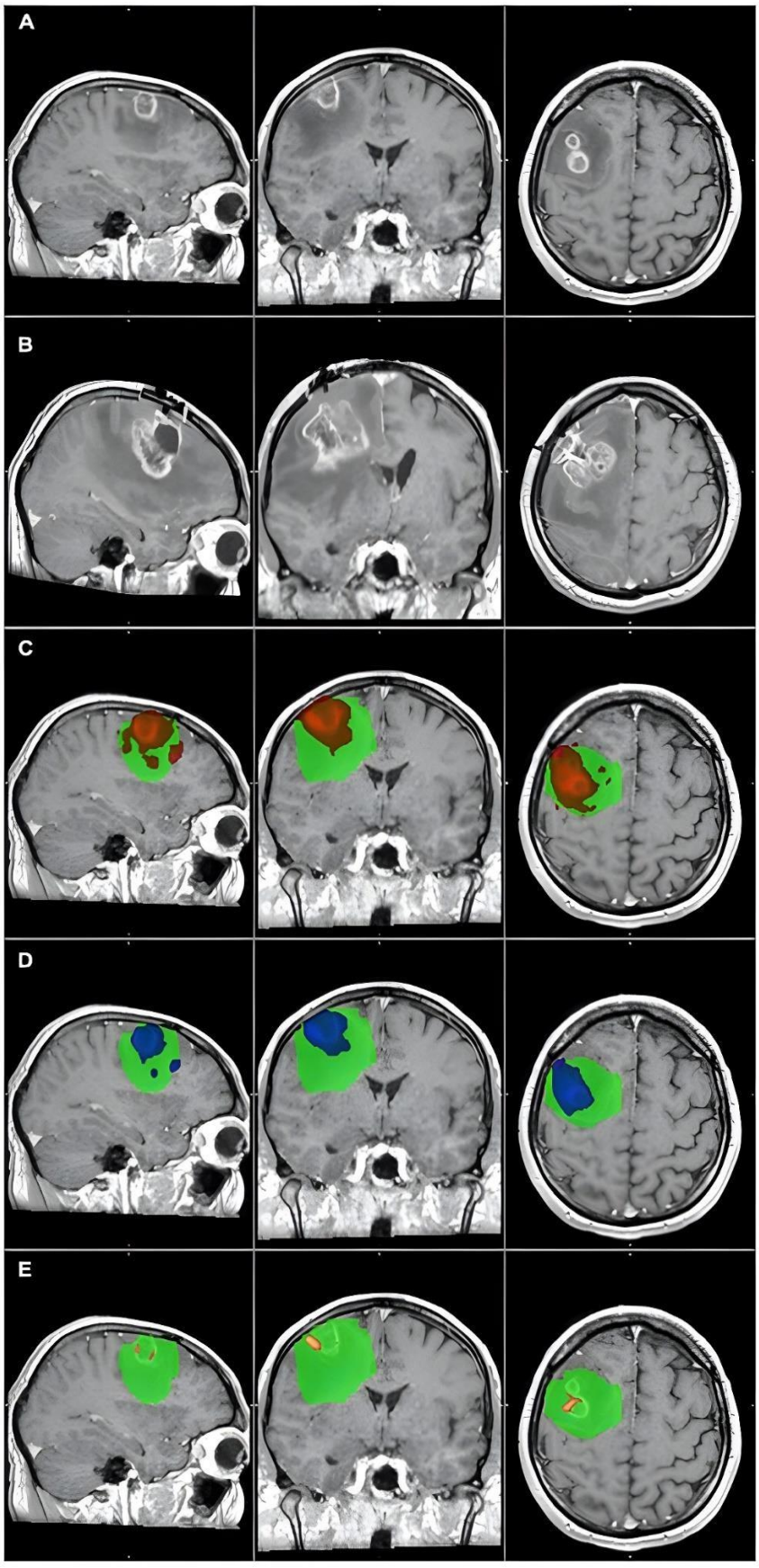

Figure 3: The primary tumor, the recurrence tumor, and the overlap between the different TCs and the tumor recurrence mask of the representative case of Patient 11 are displayed in this figure. All images are transformed to the MNI152 1 mm space. (A) The preoperative contrast enhanced T1 image. The tumor is located in the left

temporo-parietal region and does not enhance the contrast agent, but histology verified the glioblastoma. (B) The size and the location of the tumor recurrence. (C) The 1% TC (red) is overlapped on the tumor recurrence mask (green). (D) The 5% TC (blue) is overlapped on the tumor recurrence mask (green). (E) The 40% TC (red-yellow) is overlapped on the tumor recurrence mask (green). (C–E) Are on the preoperative T1 images. The main part of the recurrence is far away from the original tumor location, which leads to very low sensitivity even at the 1% threshold level.

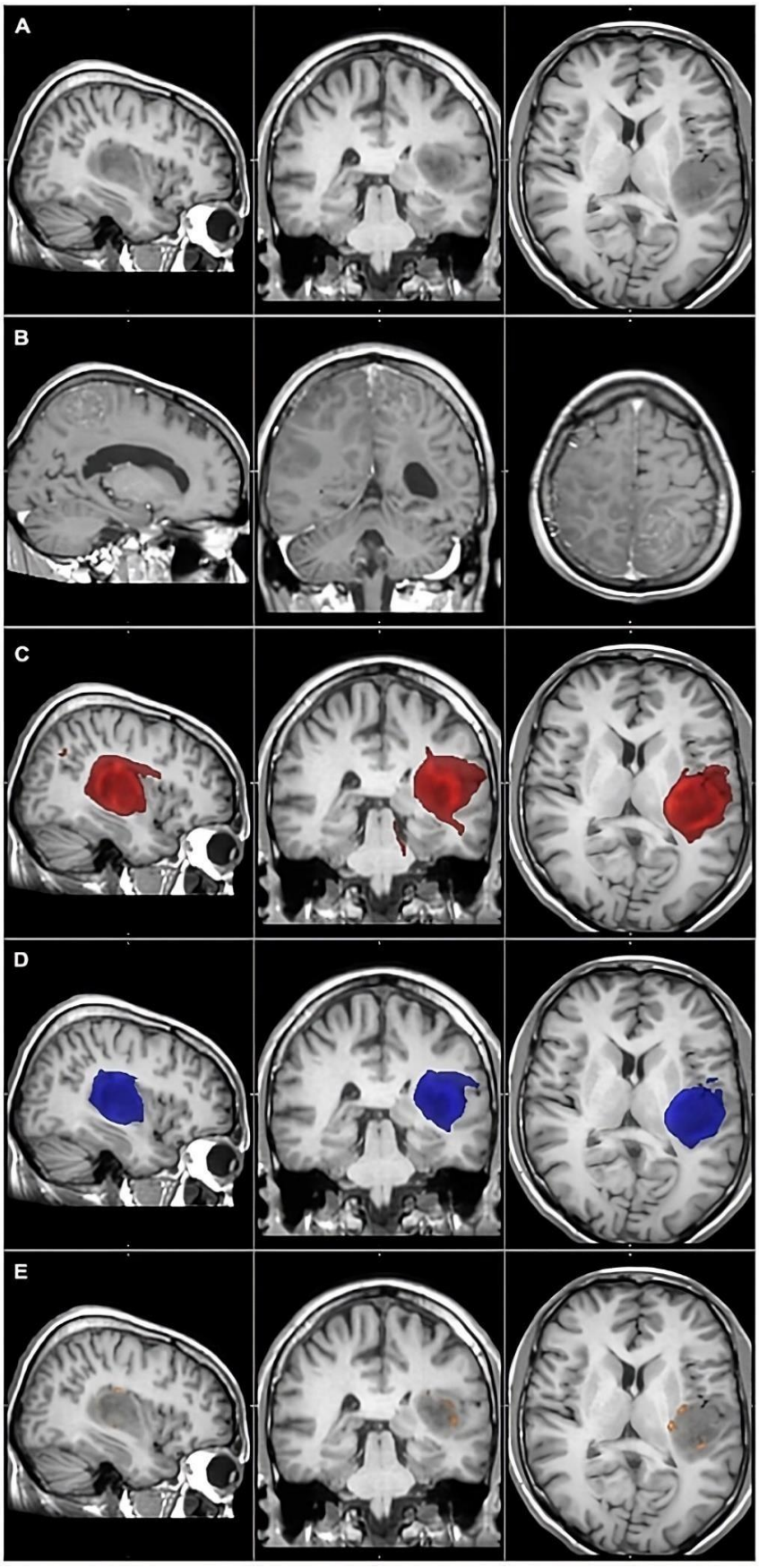

Figure 4: The primary tumor, the recurrence tumor, and the overlap between the different TCs and the tumor recurrence mask of the representative case of Patient 13 are displayed in this figure. All images are transformed to the MNI152 1 mm space. (A) The preoperative contrast enhanced T1 image. Two small tumors with ring

shaped contrast enhancement can be seen in the right frontal region. (B) The size and the location of the tumor recurrence. (C) The 1% TC (red) is overlapped on the tumor recurrence mask (green). (D) The 5% TC (blue) is overlapped on the tumor recurrence mask (green). (E) The 40% TC (red-yellow) is overlapped on the tumor recurrence mask (green). (C–E) Are on the preoperative T1 images. As it can be seen, the TCs are fully overlapping with the tumor recurrence mask and therefore the specificity is 100% at every threshold. On the other hand, the recurrence remarkably exceeds the border of the TCs, and the sensitivity is low, even at 1%. Please note that the direction of the recurrence is in correspondence with the TCs, and the low sensitivity is the result of the fast tumor progression.

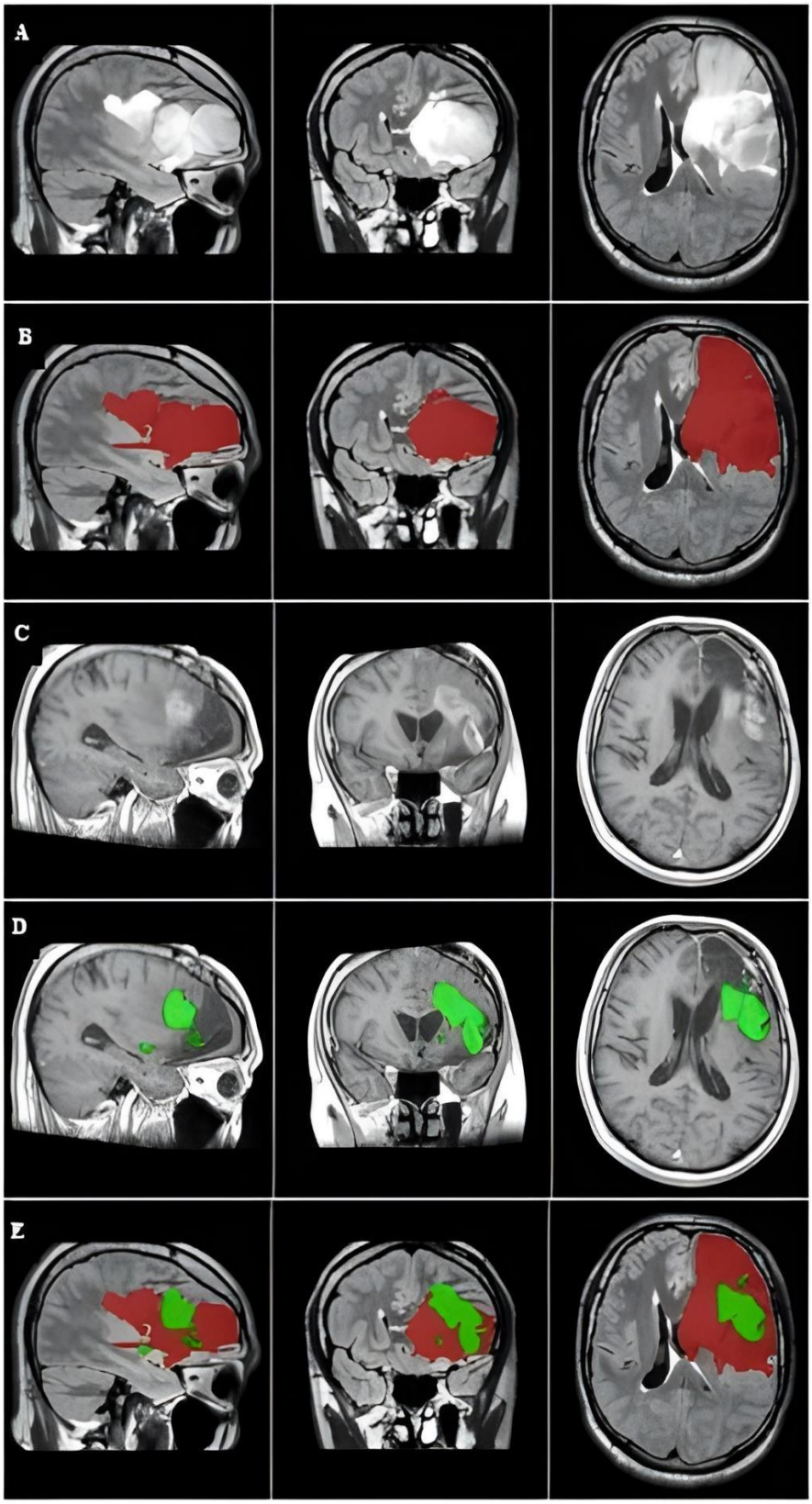

Figure 5: A representative case showing the primary tumor, tumor recurrence, and overlap between the two masks. The images were captured in the MNI152 1-mm space. (A) The primary tumor is visualized on preoperative FLAIR image of the left parietooccipital area. (B) Preoperative FLAIR mask covering the hyperintense region (red). (C) CE-T1 image shows progression of infiltrated tumor cells around the resected cavity. (D) The tumor recurrence mask covers the postcontrast-enhanced area where the tumor recurred (green). (E) Overlap between the primary tumor (red) and tumor recurrence (green).

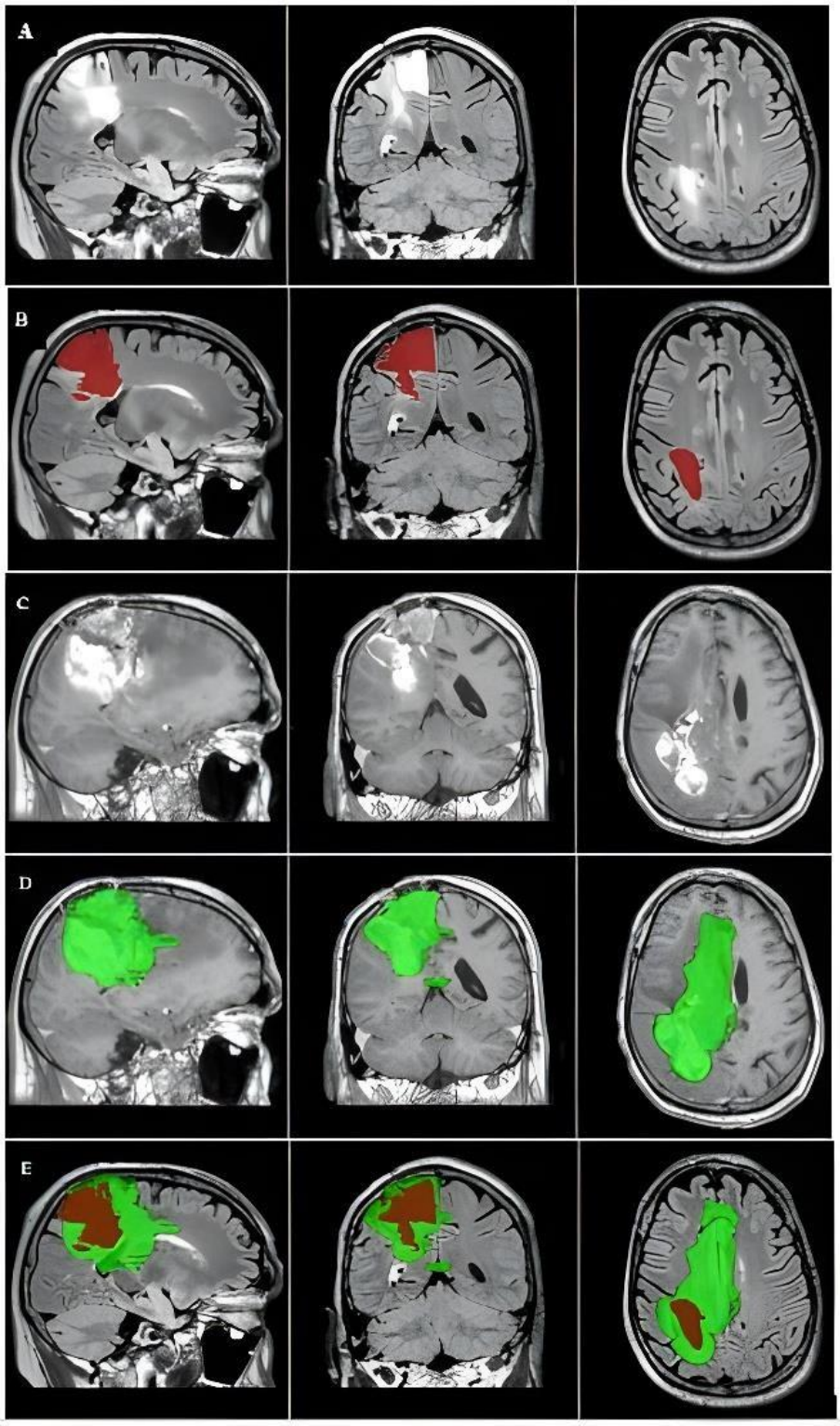

Figure 6: A representative case showing the primary tumor, tumor recurrence, and overlap between the two masks. The images were captured in the MNI152 1-mm space. (A) The primary tumor is visualized on preoperative FLAIR image of the right frontal area. (B) Primary tumor mask covers the abnormal region on the preoperative FLAIR image (red). (C) Follow-up CE-T1 shows tumor progression, with the (D) contrast-enhanced tumor recurrence mask on CE-T1 where the tumor recurred (green). (E) Shows the overlap between the primary tumor (red) and the tumor recurrence (green).

3.6 Data analysis

3.6.1 Probabilistic tractography

Probabilistic tractography was performed using the primary tumor mask as the seed region, enabling the identification of white matter pathways infiltrated by the tumor. The default settings of the FDT toolbox (5,000 samples, 0.5-mm step length, curvature threshold = 0.2) were applied, following the method described by Behrens et al. (2003a, b). This process resulted in a probabilistic tract, comprising a set of voxels with different probabilities of connection to the original seed mask. The resulting tractography output was termed “tumor connection” (TC).

To minimize low-probability connections (potential false positives), threshold levels were applied to include only those voxels with connectivity values equal to or exceeding a specific percentage of the maximum connectivity value within the TC. This approach followed methodologies which were described before (Bennett et al., 2011 and Khalsa et al., 2014).

The connectivity was defined as the total number of successful samples per voxel. Thirteen threshold levels were examined (1, 5, 10, 15, 20, 25, 30, 40, 50, 60, 70, 80, and 90%) resulting in thirteen distinct TCs (Figures 2-4). Each threshold level was evaluated to determine which one provide the highest sensitivity and specificity in predicting the true extent of the tumor.

3.6.2 Defining the affected brain areas

The preoperative CE-T1 tumor mask was only used as the seed mask for probabilistic tractography. For all latter calculations the TCs were used. For each patient, the standard cortical and subcortical brain regions were projected onto the primary tumor masks delineated on FLAIR images, the tumor recurrence masks and the TCs. It was then calculated that how many brain regions are involved and subsequently the sensitivity, specificity, positive and negative predictive value (PPV and NPV) were calculated (Figures 5 and 6).

3.6.3 Sensitivity and specificity calculations

To evaluate the predictive capability of both methods (different TCs and FLAIR tumor masks) the sensitivity, specificity, PPV, and NPV were calculated based on their overlap with the tumor recurrence mask. Because of the brain shift, mass effect and the edema, the preoperative TCs and FLAIR tumor masks and the postoperative tumor recurrence masks alignment cannot be done precisely. To overcome this limitation, we developed a special method to define the overlap. The tumor masks were overlapped on the cortical and subcortical masks and then the number of the affected cortical and subcortical regions were defined. It was then calculated that how many same and different brain regions are involved by the tumor (TCs and FLAIR tumor masks) and the recurrence masks, respectively.

The above analyzing steps were done in the standard MNI 1 mm space. This spatial normalization allowed consistent anatomical referencing across subjects.

The complete analysis pipeline - including preprocessing, mask definition, and tractography required approximately 1 hour per patient.

For each patient, sensitivity and specificity were determined at 13 different threshold levels of the tractography group. These are the tumor connections (TCs).

Sensitivity and specificity formula were as follows (Monaghan et al., 2021):

- **Sensitivity = A / (A + C)**
- **Specificity = D / (D + B)**

True Positives (A): Brain regions overlapping with both the TC (or FLAIR tumor mask) and the tumor recurrence mask.

False Positives (B): Brain regions overlapping only with the TC (or FLAIR tumor mask), but not with the tumor recurrence mask.

False Negatives (C): Brain regions overlapping only with the tumor recurrence mask, but not with the TC (or FLAIR tumor mask).

True Negatives (D): Brain regions not overlapping with either the TC (or FLAIR tumor mask) or the tumor recurrence mask.

In addition to these metrics, PPV and NPV were computed to further evaluate the predictive effectiveness of FLAIR reliability. Individual patient results and group averages were calculated and evaluated.

- **PPV= A / (A + B)**
- **NPV= D / (D + C)**

4. Results

The two retrospective studies included 20 patients whom diagnosed with high-grade glioma, classified according to the WHO 2021 criteria. The two most common neurological deficits were hemiparesis (35%) and speech disturbances (25%). Preoperatively, 40% of the patients did not exhibit severe neurological symptoms. The average Karnofesky Performance Score (KPS) was 73% preoperatively, improving to 80% at 2 months postoperatively.

All patients underwent navigation-guided, individually planned, minimally invasive craniotomy using Medtronic Inc. Stealth Station systems (iNav or S8). Total resection was achieved in 70% of cases, while subtotal resection was achieved in the remaining 30%. The progression-free survival, overall survival, age distribution, and female-to-male ratio were consistent with values reported in the literature (Ostrom and Barnholtz-Sloan, 2011; Michaelsen et al., 2018).

4.1 Probabilistic tractography

Out of 20 patients, only 18 patients' data were averaged and evaluated. The group female-to-male ratio was 1:3 (median age was 51.5 years). A total of 50% of the patients were between 45 and 60 years old. Most frequently, the tumor was located in the left hemisphere (75%) and in the frontal lobe (45%). Four patients (20%) had grade 3 anaplastic oligodendroglioma (Table 1-Appendix 1).

There were two outliers in the study group (Patients 11 and 13). These 2 patients showed remarkably lower sensitivity than the rest of the patients (Table 2, Appendix 2 and Figures 3, 4 respectively). Their results were excluded from the group analyses as it is explained in the section "Discussion."

TCs with higher threshold levels were associated with higher specificity and lower sensitivity. The maximum sensitivity and specificity were observed at 1% and 90%, respectively (Table 3, Appendix 3).

The TC with the 5% threshold level seemed to give the most reliable results. In the majority of the patients (72.2%), sensitivity was higher than 75%. Additionally, in 77.7% of patients, specificity was greater than 85%. At the group level, both measures were higher than 80%. Average sensitivity was 81% and average specificity was 90% at the 5% threshold (Table 3 and Graph 1 and Figure 2).

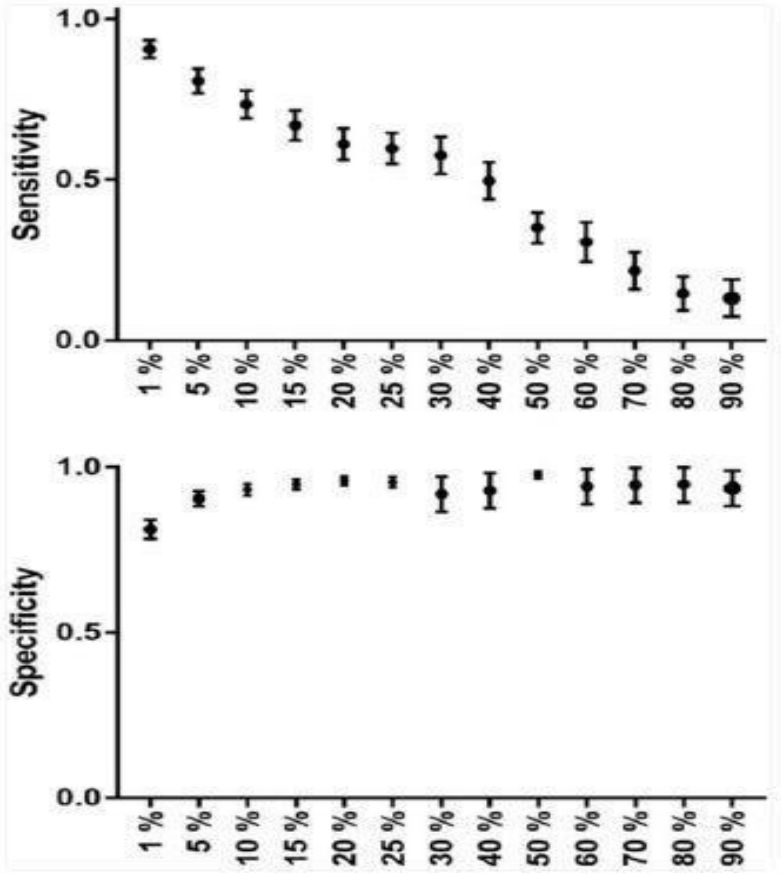

Graph 1: The group average sensitivity and specificity values (with standard error of mean) can be seen on this graph at each threshold level. Sensitivity decreases in an nearly linear fashion, while specificity has a nearly parabolic increase along the increasing threshold levels.

4.2 FLAIR

Out of 20 patients, only 16 patients' data were sufficient to be include in the study. 4 patients did not have proper quality of preoperative FLAIR images to reliable delineate the tumor mask. The female male ratio is 1:2 and the average age was 52 years. The 4 excluded patients' data have not been assessed neither individually nor at the group level calculations. Tumors were predominantly located in the left frontal lobe (50%).

Overall, the sensitivity was 82.6%, specificity was 84.7%, PPV was 50%, and NPV was 95.8%. Two patients showed high sensitivity and low specificity, and vice versa (Figures 5 and 6).

5. Discussion

Glioblastoma is widely regarded as one of the most aggressive forms of cancer, with an overall survival rate of 18 months and only 1% of patients surviving beyond 5 years after diagnosis.

The gold standard treatment involves maximal safe surgical resection, followed by oncological and radiological therapies. Studies have shown a positive correlation between the extent of primary tumor removal and improved overall survival rates (Wykes et al., 2021).

In oncological surgery, an extended safety margin is used to remove the primary tumor and all the infiltrated surrounding tissues. Unfortunately, this approach cannot be employed in the case of primary brain tumors. Resection should be limited to the tumor mass-normal tissue border (Yasargil, 1994). The removal of healthy brain tissue is likely to cause severe neurological symptoms and a reduced quality of life. The remaining tumor cells infiltrating the normal brain tissue should be treated with oncological procedures, such as irradiation and chemotherapy (Stupp et al., 2005).

Glioblastoma, which is the most aggressive type of these infiltrative primary brain tumors, recurs from the remaining infiltrative tumor cells (Petrecca et al., 2013). Currently, the radiological modality with the highest sensitivity for glioblastoma is MRI (Shukla et al., 2017). The tumor mass is visible on the contrast-enhanced T1 images, but the cells infiltrating the otherwise normal brain tissue (which can be at a distance of several centimeters from the contrast enhancing border) are not.

Theoretically, if the true extent of the glioblastoma can be revealed, prolonged progression-free and overall survival periods can be achieved with supratotal resection and individually planned radiation therapy. Probabilistic tractography has the advantage that its result can be thresholded, and not like on FLAIR, the false positive results can be ruled out.

In the recent decade, FLAIR, MRS and amino acid based PET-CT were introduced to identify the true extent of glioblastoma as potential imaging modalities. In case of glioblastoma, the hyperintense volume in the FLAIR images corresponds to microscopic tumor infiltration and edema, and usually exceeds the contrast enhancing volume (Watanabe et al., 1992). Preoperative FLAIR images can be used to plan surgical resection and irradiation therapy but there is no clear evidence that it has a positive prognostic value (Garrett et al., 2017; Altieri et al., 2019). The extent of FLAIR signal hyperintensity prior to the initial surgery is not associated with survival.

On the other hand, overall survival significantly affected by the preoperative contrast enhancement volume (Altieri et al., 2019). In addition, FLAIR images can identify tumor progression earlier than contrast enhanced T1 on the follow-up MRI and associated with progression free and overall survival (Garrett et al., 2017). It is hard or even impossible to differentiate where microscopic tumor infiltration ends within the edema. Identifying the exact borders of the infiltrative part of the glioblastoma is challenging on FLAIR. Therefore, the true extent of the tumor can be overestimated due to false positive hyperintense regions.

Magnetic resonance spectroscopy has promising results to predict the site of glioblastoma recurrence. In one study, MRS has 88.8% sensitivity and 97.6% specificity to detect tumor vs. normal brain tissue and 71% true and 10% false positive ratio to predict the site of glioblastoma recurrence (Deviers et al., 2014). The spatial resolution of MRS was very low (6.25 mm _ 6.25 mm _ 25.0 mm = 976,5 mm3) in this study (Ken et al., 2013). These factors make it challenging to use MRS results in routine patient care and image guided surgical and radiation therapy. Diffusion MRI based tractography on the other hand has much better resolution, which makes it a more feasible method.

^{11}C-Methionin, ^{18}F-DOPA, and ^{18}F-FET-PET have been introduced for primary and secondary brain tumor detection. The increased uptake in brain tumors is based on the overexpression of the amino acid transporter in the tumor cells and in the tumor supplying vessels, which is independent from the blood-brain barrier (BBB). Therefore, these aminoacid based PET methods are appropriate for the following goals: to help differentiate necrosis and tumors, provide information on changed biochemical processes prior to the appearance of morphological changes, and to characterize the residual brain tumor volume for more accurate post-operative radiotherapy.

^{18}F-FET-PET has been used in some studies to determine the tumor and/or residual tumor volume for radiotherapy. In most cases, the target volume for irradiation determined this way was larger than the one determined with MRI alone (Munck Af Rosenschold et al., 2015). Postoperative ^{18}F-FETPET scans had a higher sensitivity for detecting residual tumor than MRI (Buchmann et al., 2016). Nonetheless, ^{18}F-FET-PET had a sensitivity of 87% and a specificity of 68% for detecting glial tumors (Hutterer et al., 2013). These results make ^{18}FFET- PET a potential diagnostic tool to identify the true extent of glioblastomas.

^{18}F-FET-PET have several disadvantages that make its routine clinical use difficult. It is quite expensive, time consuming (the total examination time can be several hours), and

exposes the patient to radiation. Additionally, spatial resolution is limited to 5 mm.

MRI, on the other hand, uses no radiation, has high spatial resolution (<1 mm), and takes about 15–20 min. It is also a part of the standard diagnostic protocol for glioblastoma and therefore does not require any extra procedures. If an MRI modality that is suitable for identifying the true extent of glioblastomas could be found, it would be a much more feasible examination to be used in clinical practice than ^{18}F-FET-PET (Muoio et al., 2018).

Tractography is an advanced MRI imaging modality. It is based on diffusion MRI images. The direction of the diffusion movement of water molecules in the brain can be reconstructed. In the white matter, this movement tends to be parallel to the fiber tract orientation. Using this information, white matter pathways can be reconstructed mathematically. The major drawback of tractography is that the diffusion direction can be uncertain in several important brain regions (e.g., white and gray matter border, gray matter, basal ganglia, crossing fiber tracts, tumor, peritumoral edema) and, therefore, the result is unreliable (Bammer, 2003; Wakana et al., 2004; Johansen-Berg and Behrens, 2006). Probabilistic tractography is one possible algorithm to overcome this limitation. It takes the uncertainty of water diffusion into account. The result of probabilistic tractography is a set of voxels. Each voxel has a value representing the probability that the given voxel belongs to the visualized white matter fiber tract. This basically means that all voxels can be identified, even the ones that have the lowest chance of being connected to the tract. It also means that there are a lot of false positive results. Therefore, an optimal threshold level must be defined to exclude the highest number of false positive and false negative voxels.

Glioblastoma originates from a core. As it progresses, a tumor mass and an infiltrative part of the tumor develop (Wick et al., 2018). Due to the fast-growing nature of the tumor, the center of the mass is often necrotized, and the edges consist of viable tumor (Young, 2007). The infiltrative part is a mixture of tumor cells and white matter fiber tracts. The two parts form a structural unit and can be considered an abnormal fiber tract that has several connections with the surrounding pathways (Osswald et al., 2015). This makes probabilistic tractography a potential tool to identify the connections between the tumor and its pathways, furthermore, the infiltrated brain regions and, more importantly, the true extent of the tumor could be pinpointed (Mukherjee et al., 2008).

The problem is that when probabilistic tractography is performed, the infiltrative tumor part is invisible on standard MRI images (Lasocki and Gaillard, 2019).

When the remaining tumor cells become resistant to the oncological treatment, they start to proliferate (Milano et al., 2010; Petrecca et al., 2013). The infiltrative part increases in volume and then becomes visible on conventional MRI images. Intuitively, the tumor becomes visible in the brain regions where it was invisible on the initial and previous follow-up images. The identified tumor recurrence then can be used for comparison with the TCs identified using probabilistic tractography.

We had to find a method that would allow us to reliably compare the TCs with the tumor recurrence mask. It would be a simple way to define the overlapping volume of the two and then, based on the ratio of the overlap, calculate sensitivity and specificity. Unfortunately, this method would not give us a reliable result because of the following two limiting factors. First, in most of the cases, the anatomy of the brain gradually changes during the time between the preoperative and the follow-up MRI scan. It is challenging, even with non-linear registration, to create perfect alignment between the preoperative and follow-up MRI images because of the mass effect of the tumor. Therefore, a direct comparison of the anatomical location of the TCs and the tumor recurrence mask is unreliable. The second limitation is due to the nature of tractography and the natural course of glioblastomas. TC volumes change by thresholding. The recurrence volume depends on when the follow-up MRI scan was performed. Contrast enhancement first appears along the fiber tracts, then the tumor gets thicker and soon exceeds the volume of the fiber tract. Accordingly, infiltrated fiber tracts may be visible on the tractography images, but the volume may differ remarkably from the tumor recurrence mask.

Therefore, instead of using the volumes for comparison, we identified brain regions affected by both the tumor and the TCs. According to the JHU ICBM–DTI–81 white matter label and AAL3 standard atlases, the standard brain was divided into subcortical and cortical regions, and the number of affected regions was calculated.

At the group level, we found high sensitivity (81%) and specificity (90%) rates at the 5% threshold level. Our results suggest that the presented method is a reliable and clinically feasible way to predict the true extent of glioblastomas.

On the other hand, there are several limiting factors of this method that can affect the final result.

As it has been previously mentioned the preoperative and follow-up MRI images do not align perfectly with the standard MRI images. This means that the TCs and the tumor recurrence mask are not completely in an anatomically identical location. This problem

cannot be completely eliminated by neither of the widely available registration algorithms. The misalignment can only be minimized to have the least effect on the results (Kocher et al., 2021).

To overcome these two limitations, we did not make a direct comparison between the volumes of the TCs and the tumor recurrence mask but counted the number of affected cortical and subcortical areas within the standard space. Registering the preoperative and follow-up MRI images to the standard space reduces the anatomical distortion between the two to the possible minimum. Even if the TCs and the tumor recurrence mask are in an anatomically identical location, the volume difference between the two can change the results. Therefore, we did not compare the volumes but the number of the affected brain areas instead. This way, if either the TC or the tumor recurrence mask reached one area, it was counted as positive. The difference in the volumes reaching the same location did not matter. Only the positive hit counts. Unfortunately, even this technique cannot perfectly rule out the above mentioned limitations. A good example for this is the case of Patient 13 (see below).

There was another limitation to the presented method, which is related to the nature of the tumor recurrence. The two outlier patients are perfect examples to that. The appearance of the recurrence on the follow-up MRI was not eligible to determine which part of the brain was infiltrated preoperatively. In their case, the presented method was unreliable to define the specificity and sensitivity. Their data were excluded from the group average to avoid false distortion of the results.

Patient 11 had a rare type of tumor progression. The recurrence appeared in a multifocal fashion, far away from the original site (Figure 3).

Patient 13 had a recurrence in the white matter around the resection cavity. The contrast enhancing part of the original tumor was very small (6.2 cm3) if compared to the recurrence volume (54.9 cm3). A huge area of the frontal lobe was included by the tumor recurrence mask but not by TCs (Figure 4), and there was a considerable difference in the number of affected brain regions.

In both cases, the special anatomical situations mentioned above resulted in a low level of overlap between the TCs and the tumor recurrence masks, therefore they decreased the sensitivities. In the case of Patient 11, the distant infiltrated areas could not be identified based on the tractography images, and the low sensitivity value was real. However, in the case of Patient 13, it was a partially false result. At the time of the follow-up MRI tumor progression was significant. The TCs overlapped with several brain regions where the recurrence appeared, and the direction of the recurrence was in concordance with the TCs.

On the other hand, the tumor recurrence also contained many brain regions away from the original site. This resulted in a high number of false negative results and low sensitivity, even though tractography predicted the location of the recurrence well. The case of Patient 13 enlightens the importance of the timing of the follow-up MRI in our methodology. An earlier follow-up MRI with a less prominent tumor progression may have resulted in a better correlation with the TCs. In conclusion we believe that in the case of Patient 13, the TC with the 5% threshold level would give us reliable information regarding the true extent of the tumor, but because of the reason discussed above, the calculate sensitivity is low (Table 2 and Figure 4).

On the other hand, the two outlier patients also highlight the limitation of the applicability of the presented method. It provides useful information in only those glioblastoma patients who have typical progression pattern and the recurrence appears within the close proximity of the resection cavity. According to the literature 90–95% of the patients belongs to that group (De Bonis et al., 2013). Our study group is in concordance with that, as 90% of the patients had the recurrence around the resection cavity.

As it was mentioned above FLAIR is more frequently used to identify not only the contrast enhancing but the infiltrative tumor part also, however the significance of it on patient survival is not clear (Garrett et al., 2017; Altieri et al., 2019).

We wanted to examine if FLAIR has the same potential to identify the tumorous infiltration in glioblastoma patients as probabilistic tractography. Using FLAIR images would be a more convenient way in clinical practice as it does not need advanced postprocessing. We applied the same method to the same patient population group as in the tractography study. There was a minor change in the pipeline as instead of the TCs, the preoperative tumor mask was used which was delineated on the FLAIR images.

As a result of the study, we found that the FLAIR images have an overall sensitivity and specificity at 82.6% and 84.7% respectively. Although our study demonstrated high sensitivity and specificity, when we performed the direct visual control, remarkable discrepancies were revealed between the tumor and recurrence masks. It could be due to the reason that FLAIR images did not provide a clear estimation of the true false negative to true false positive ratio because the method does not distinguish accurately between tumoral and non-tumoral areas, such as edema. In glioblastoma surgery, the ratio of these factors are crucial because overestimating the extent of tumor resection may cause severe neurological impairments, whereas missing diseased tissues directly affects survival.

Therefore, additional statistical method was needed to validate our theory.

PPV and NPV are defined to reflect the proportions of true positive and negative results (Monaghan et al, 2021). At the group level the PPV was 50.2% and the NPV was 95.8%. These numbers indicate that although FLAIR images are highly reliable to rule out most of the nontumoral tissues (high NPV, specificity and sensitivity), it has a low accuracy to confirm the presence of infiltrating tumor cells (low PPV) and therefore the true extent of glioblastoma. This discrepancy is likely due to the relatively high false-positive results, which overestimated the tumor extent.

We would like to present two representative cases to demonstrate the contradicting results of the FLAIR study.

In the first representative case (Patient 3, Figure 5), the high sensitivity implied that most of the brain regions covered by the primary tumor mask were true cancerous tissues. This case supports the previously proposed reports that FLAIR imaging is very sensitive for assessing tumor cell proliferation. However, according to the literatures the hyperintense region on FLAIR may overestimate tumor boundaries by reflecting other factors, such as, edema, potentially leading to inaccuracies in diagnostic or treatment planning.

In contrast, the second representative case (Patient 4, Figure 6) exhibited considerably higher specificity than sensitivity. Compared with the original tumor mass, the significantly larger area covered by the tumor recurrence mask indicated that the majority of the brain regions left undetected by the preoperative FLAIR tumor mask were, in fact, infiltrated by cancer cells that had spread into the surrounding tissue, ultimately led to rapid tumor progression, resulting in poor overall survival.

This study highlighted both the strengths and the limitations of preoperative FLAIR imaging in predicting glioblastoma propagation. While hyperintensity in FLAIR images can visualize abnormal regions, it cannot accurately and reliably detect microscopic infiltrative tumor cells.

Strictly relying on FLAIR images can negatively affect the glioblastoma patients' survival.

However, our results are promising the study had several limitations, such as inaccuracy of manual delineation of the tumor masks, imperfect registration and potential misalignment, and of course the small sample size. Future studies incorporating a larger sample size and addressing the aforementioned limitations may lead to more reliable calculations.

6. Conclusion

In the both studies, we presented two distinct approaches to identify the true extent of glioblastomas at the time of diagnosis. The probabilistic tractography-based method enabled us to visualize the infiltrated brain areas with high sensitivity and specificity in most patients, which may support more radical tumor resection and personalized radiation therapy planning which can potentially leading to prolonged survival. FLAIR images on the other hand showed high reliability to identify the unaffected brain but low reliability to visualize the infiltrative glioblastoma part. Therefore, it is not advised to use FLAIR solely for surgical resection planning as it can result in overestimated tumor size and unnecessarily high risk of surgery. At the same time FLAIR is a good MRI modality for irradiation planning alongside the contrast enhanced T1. According to our results we recommend incorporating DTI based probabilistic tractography and FLAIR into the MRI imaging protocol of glioblastoma to provide individual treatment options and better survival for the patients.

List of abbreviations

AAL3
Automated anatomical labeling atlas 3
ASSET
Array coil spatial sensitivity encoding
BEDPOSTX
Bayesian estimation of diffusion parameters obtained using sampling techniques
DICOM
Digital imaging and communications in medicine
DTI
Diffusion tensor imaging
DWI
Diffusion weighted images
F-DOPA
Fluoro-dihydroxyphenylalanine
F-FET
F-Fluoro-Ethyl-Tyrosine
FDT
FMRIB's diffusion toolbox
FLAIR
Fluid-attenuation inversion recovery
FMRIB
Functional magnetic resonance imaging of the brain
FOV
Field of view
FSL
FMRIB software library
FSPGR
Fast spoiled gradient echo
GE
General electric
GPU
Graphical processing unit
IDH
Isocitrate dehydrogenase mutation
JHU-ICMB-DTI
Johns Hopkins University, international consortium of brain mapping, diffusion tensor imaging
LNR
Lactate/N-acetylaspartate ratio
MGMT
O^6-methylguanine-DNA methyltransferase
MNI152
Montreal neurological institute 152
MRI
Magnetic resonance imaging
MRS
Magnetic resonance spectroscopy
NIFTI
Neuroimaging informatics technology initiative
OS
Overall survival
PET-CT
Positron emission tomography, computed tomography
PFS
Progression free survival
PROBTRACX
Probabilistic tracking with crossing fibers
SWI
Susceptibility weighted images
TC
Tumor connection
TE
Time of echo
TR
Time of repetition.

References

1. Ahmed, F. I., Abdullah, K. G., Durgin, J., Salinas, R. D., O'Rourke, D. M., and Brem, S. (2019). Evaluating the Association Between the Extent of Resection and Survival in Gliosarcoma. Cureus 11:e4374.
2. Altieri, R., Melcarne, A., Soffietti, R., Rudá, R., Franchino, F., Pellerino, A., et al. (2019). Supratotal Resection of Glioblastoma: Is Less More? Surg. Technol. Int. 10, 432–440.
3. Andersson, J. L. R., and Sotiropoulos, S. N., (2016). An integrated approach to correction for off-resonance effects and subject movement in diffusion MR imaging. NeuroImage 125, 1063–1078.
4. Aydin, H., Sillenberg, I., Von Lieven, H. Patterns of failure following CT-based 3-D irradiation for malignant glioma. Strahlenther. Onkol. 2001; 177:424–431.
5. Bammer, R. (2003). Basic principles of diffusion-weighted imaging. Eur. J. Radiol. 45, 169–184.
6. Barani, I. J., and Larson, D. A. (2015). Radiation therapy of glioblastoma. Cancer Treat. Res. 163, 49–73.
7. Bauchet, L., Mathieu-Daudé, H., Fabbro-Peray, P., Rigau, V., Fabbro, M., Chinot, O., et al. (2010). Oncological patterns of care and outcome for 952 patients with newly diagnosed glioblastoma in 2004. Neuro Oncol. 12, 725–735. doi: 10.1093/neuonc/noq030
8. Behrens, T. E. J., Berg, H. J., Jbabdi, S., Rushworth, M. F. S., and Woolrich, M. W. (2007). Probabilistic diffusion tractography with multiple fibre orientations: What can we gain? Neuroimage 34, 144–155.
9. Behrens, T. E. J., Johansen-Berg, H., Woolrich, M. W., Smith, S. M., Wheeler-Kingshott, C. A. M., Boulby, P. A., et al. (2003a). Non-invasive mapping of connections between human thalamus and cortex using diffusion imaging. Nat. Neurosci. 6, 750–757.
10. Behrens, T. E. J., Woolrich, M. W., Jenkinson, M., Johansen-Berg, H., Nunes, R. G., Clare, S., et al. (2003b). Characterization and propagation of uncertainty in diffusion-weighted MR imaging. Magn. Reson. Med. 50, 1077–1088.
11. Bennett, I. J., Madden, D. J., Vaidya, C. J., Howard, J. H. J., and Howard, D. V. (2011). White matter integrity correlates of implicit sequence learning in healthy aging. Neurobiol. Aging 32, 2317.e1–12.

12. Brandes, A. A., Tosoni, A., Franceschi, E., Sotti, G., Frezza, G., Amistà, P., et al. Recurrence pattern after temozolomide concomitant with and adjuvant to radiotherapy in newly diagnosed patients with glioblastoma: Correlation With MGMT promoter methylation 456 status. J. Clin. Oncol.27:1275–1279.
13. Buchmann, N., Kläsner, B., Gempt, J., Bauer, J. S., Pyka, T., Delbridge, C., et al. (2016). (18)F- fluoroethyl-l-thyrosine positron emission tomography to delineate tumor residuals after glioblastoma resection: A comparison with standard postoperative magnetic resonance imaging. World Neurosurg. 89, 420– 426. doi: 10.1016/j.wneu.2016.02.032
14. Certo, F., Stummer, W., Farah, J.O., Freyschlag,, C., Visocchi, M., Morrone, A, et al. (3029). Supramarginal resection of glioblastoma: 5-ALA fluorescence, combined intraoperative strategies and correlation with survival. J Neurosurg Sci. 63(6):625-632.
15. Cha, S. Neuroimaging in Neuro-Oncology. Neurotherapeutics. 2009; 6(3):465-77.
16. Costabile, J. D., Alaswad, E., D'Souza, S., Thompson, J. A., and Ormond, D. R. (2019). Current Applications of Diffusion Tensor Imaging and Tractography in Intracranial Tumor Resection. Front. Oncol. 9:426.
17. De Bonis, P., Anile, C., Pompucci, A., Fiorentino, A., Balducci, M., Chiesa, S., et al. (2013). The influence of surgery on recurrence pattern of glioblastoma. Clin. Neurol. Neurosurg. 115, 37–43.
18. de Leeuw, C. N., and Vogelbaum, M. A. (2019). Supratotal resection in glioma: A systematic review. Neuro Oncol. 21, 179–188.
19. Demuth, T., and Berens, M. E. (2004). Molecular mechanisms of glioma cell migration and invasion. J. Neurooncol. 70, 217–228.
20. Deviers, A., Ken, S., Filleron, T., Rowland, B., Laruelo, A., Catalaa, I., et al. (2014). Evaluation of the lactate-to-N-acetyl-aspartate ratio defined with magnetic resonance spectroscopic imaging before radiation therapy as a new predictive marker of the site of relapse in patients with glioblastoma multiforme. Int. J. Radiat. Oncol. Biol. Phys. 90, 385–393.
21. Garrett, M. D., Yanagihara, T. K., Yeh, R., McKhann, G. M., Sisti, M. B., Bruce, J. N., et al. (2017). Monitoring Radiation Treatment Effects in Glioblastoma: FLAIR Volume as Significant Predictor of Survival. Tomography 3, 131–137.
22. Haddad, A. F., Young, J. S., Morshed, R. A., Berger, M. S. FLAIRectomy: Resecting beyond the Contrast Margin for Glioblastoma. Brain Sci. 2022; 12(5):544.

23. Hua, K., Zhang, J., Wakana, S., Jiang, H., Li, X., Reich, D. S., et al. (2008). Tract probability maps in stereotaxic spaces: Analyses of white matter anatomy and tract-specific quantification. Neuroimage 39, 336–347.
24. Hutterer, M., Nowosielski, M., Putzer, D., Jansen, N. L., Seiz, M., Schocke, M., et al. (2013). [18F]-fluoro-ethyl-L-tyrosine PET: A valuable diagnostic tool in neuro-oncology, but not all that glitters is glioma. Neurooncology 15, 341–351.
25. Jenkinson, M., and Smith, S. (2001). A global optimisation method for robust affine registration of brain images. Med. Image Anal. 5, 143–156.
26. Jenkinson, M., Bannister, P., Brady, M., and Smith, S. (2002). Improved optimization for the robust and accurate linear registration and motion correction of brain images. Neuroimage 17, 825–841.
27. Johansen-Berg, H., and Behrens, T. E. J. (2006). Just pretty pictures? What diffusion tractography can add in clinical neuroscience. Curr. Opin. Neurol. 19, 379–385.
28. Ken, S., Vieillevigne, L., Franceries, X., Simon, L., Supper, C., Lotterie, J. A., et al. (2013). Integration method of 3D MR spectroscopy into treatment planning system for glioblastoma IMRT dose painting with integrated simultaneous boost. Radiation Oncology 8(1):1.
29. Khalsa, S., Mayhew, S. D., Chechlacz, M., Bagary, M., and Bagshaw, A. P. (2014). The structural and functional connectivity of the posterior cingulate cortex: Comparison between deterministic and probabilistic tractography for the investigation of structure-function relationships. Neuroimage 102, 118–127.
30. Kis, D., Máté, A., Kincses, Z. T., Vörös, E., and Barzó, P. (2014). The role of probabilistic tractography in the surgical treatment of thalamic gliomas. Neurosurgery 10, 262–272.
31. Kis, D., Szivos, L., Rekecki, M., Shukir, B., Mate, A., Hideghety, K., et al. Predicting the true extent of glioblastoma based on probabilistic tractography. (2022). Front Neurosci. 16:886465.
32. Kocher, M., Jockwitz, C., Lohmann, P., Stoffels, G., Filss, C., Mottaghy, F. M., et al. (2021). Lesion-Function Analysis from Multimodal Imaging and Normative Brain Atlases for Prediction of Cognitive Deficits in Glioma Patients. Cancers 13:2373.
33. Lacroix, M., Abi-Said, D., Fourney, D. R., Gokaslan, Z. L., Shi, W., DeMonte, F., et al. (2001). A multivariate analysis of 416 patients with glioblastoma multiforme: Prognosis, extent of resection, and survival. J. Neurosurg. 95, 190–198.

34. Lasocki, A., and Gaillard, F. (2019). Non-Contrast-Enhancing Tumor: A New Frontier in Glioblastoma Research. AJNR. Am. J. Neuroradiol. 40, 758–765.
35. Le Bihan, D., Turner, R., Douek, P., and Patronas, N. (1992). Diffusion MR imaging: Clinical applications. AJR 159, 591–599.
36. Leemans, A., and Jones, D. K. (2009). The B-matrix must be rotated when correcting for subject motion in DTI data. Magn. Reson. Med. 61, 1336–1349.
37. Lemee, J. M., Clavreul, A., and Menei, P. (2015). Intratumoral heterogeneity in glioblastoma: Don't forget the peritumoral brain zone. Neuro Oncol. 17, 1322–1332.
38. Li, Y. M., Suki, D., Hess, K., Sawaya, R. (2016). The influence of maximum safe resection of glioblastoma on survival in 1229 patients: can we do better than gross-total resection? J Neurosurg. 2; 124(4):977-88.
39. Louis, D. N., Perry, A., Wesseling, P., Brat, D. J., Cree, I. A., Figarella-Branger, D., et al. (2021). The 2021 WHO Classification of Tumors of the Central Nervous System: A summary. Neuro Oncol. 23, 1231–1251.
40. Mascalchi, M., Filippi, M., Floris, R., Fonda, C., Gasparotti, R., and Villari, N. (2005). Diffusion-weightedMRof the brain: Methodology and clinical application. Radiol. Med. 109, 155–197.
41. Michaelsen, S. R., Urup, T., Olsen, L. R., Broholm, H., Lassen, U., and Poulsen, H. S. (2018). Molecular profiling of short-term and long-term surviving patients identifies CD34mRNA level as prognostic for glioblastoma survival. J. Neurooncol. 137, 533-542.
42. Milano, M. T., Okunieff, P., Donatello, R. S., Mohile, N. A., Sul, J., Walter, K. A., et al. (2010). Patterns and timing of recurrence after temozolomide-based chemoradiation for glioblastoma. Int. J. Radiat. Oncol. Biol. Phys. 78, 1147–1155.
43. Monaghan, T. F., Rahman, S. N., Agudelo, C. W., Wein, A. J., Lazar, J. M., Everaert, K., et al. (2021). Foundational Statistical Principles in Medical Research: Sensitivity, Specificity, Positive Predictive Value, and Negative Predictive Value. Medicina(Kaunas).57(5):503.
44. Mori, S., and van Zijl, P. C. M. (2002). Fiber tracking: Principles and strategies - a technical review. NMR Biomed. 15, 468–480.
45. Mori, S., Oishi, K., Jiang, H., Jiang, L., Li, X., Akhter, K., et al. (2008). Stereotaxic white matter atlas based on diffusion tensor imaging in an ICBM template. Neuroimage 40, 570–582.

46. Mukherjee, P., Berman, J. I., Chung, S. W., Hess, C. P., and Henry, R. G. (2008). Diffusion tensor MR imaging and fiber tractography: Theoretic underpinnings. AJNR. Am. J. Neuroradiol. 29, 632–641.
47. Munck Af Rosenschold, P., Costa, J., Engelholm, S. A., Lundemann, M. J., Law, I., Ohlhues, L., et al. (2015). Impact of [18F]-fluoro-ethyl-tyrosine PET imaging on target definition for radiation therapy of high-grade glioma. Neurooncology 17, 757–763.
48. Muoio, B., Giovanella, L., and Treglia, G. (2018). Recent Developments of 18FFET PET in Neuro-oncology. Curr. Med. Chem. 25, 3061–3073.
49. Osswald, M., Jung, E., Sahm, F., Solecki, G., Venkataramani, V., Blaes, J., et al. (2015). Brain tumour cells interconnect to a functional and resistant network. Nature 528, 93–98.
50. Ostrom, Q. T., and Barnholtz-Sloan, J. S. (2011). Current state of our knowledge on brain tumor epidemiology. Curr. Neurol. Neurosci. Rep. 11, 329–335.
51. Ostrom, Q. T., Cioffi, G., Waite, K., Kruchko, C., and Barnholtz-Sloan, J. S. (2021). CBTRUS Statistical Report: Primary Brain and Other Central Nervous System Tumors Diagnosed in the United States in 2014-2018. Neuro Oncol. 23:iii1–iii105.
52. Petrecca, K., Guiot, M. C., Panet-Raymond, V., and Souhami, L. (2013). Failure pattern following complete resection plus radiotherapy and temozolomide is at the resection margin in patients with glioblastoma. J. Neurooncol. 111, 19–23.
53. Quan G. M., Zheng Y. L., Yuan T, Lei J. M. Increasing FLAIR signal intensity in the postoperative cavity predicts progression in gross-total resected high-grade gliomas. J Neurooncol. 2018; 137(3):631-638.
54. Rapp M., Baernreuther J., Turowski B., Steiger H. J., Sabel M., Kamp M. A. Recurrence Pattern Analysis of Primary Glioblastoma. World Neurosurg. 2017; 103:733–740.
55. Roelz, R., Strohmaier, D., Jabbarli, R., Kraeutle, R., Egger, K., Coenen, V. A., et al. (2016). Residual Tumor Volume as Best Outcome Predictor in Low Grade Glioma-A Nine-Years Near-Randomized Survey of Surgery vs. Biopsy. Sci. Rep. 6:32286.
56. Rolls, E. T., Huang, C. C., Lin, C. P., Feng, J., and Joliot, M. (2020). Automated anatomical labelling atlas 3. Neuroimage 206:116189.
57. Rorden, C., Karnath, H.-O., and Bonilha, L. (2007). Improving lesionsymptom mapping. J. Cogn. Neurosci. 19, 1081–1088.
58. Sanai N., Polley M. Y., McDermott M. W., Parsa A. T., Berger M. S. An extent of resection threshold for newly diagnosed glioblastomas. J Neurosurg. 2011; 115(1):3-8.

59. Sarbu N., Oleaga L., Valduvieco I., Pujol T., Berenguer J. Increased signal intensity in FLAIR sequences in the resection cavity can predict progression and progression-free survival in gliomas. Neurocirugia (Astur). 2016; 27(6):269-276.
60. Shukla, G., Alexander, G. S., Bakas, S., Nikam, R., Talekar, K., and Palmer, J. D. (2017). Advanced magnetic resonance imaging in glioblastoma: A review. Chin. Clin. Oncol. 6:40.
61. Smith, S. M. (2002). Fast robust automated brain extraction. Hum. Brain Mapp. 17, 143–155.
62. Stupp, R., Mason, W. P., van den Bent, M. J., Weller, M., Fisher, B., Taphoorn, M. J., et al. (2005). Radiotherapy plus concomitant and adjuvant temozolomide for glioblastoma. N. Engl. J. Med. 352, 987–996.
63. Tonn, J. C., and Goldbrunner, R. (2003). Mechanisms of glioma cell invasion. Acta Neurochir. Suppl. 88, 163–167.
64. Stummer W., Pichlmeier U., Meinel T., Wiestler O. D., Zanella F., Reulen H. J. Fluorescence-guided surgery with 5-aminolevulinic acid for resection of malignant glioma: A randomised controlled multicentre phase III trial. Lancet Oncol. 2006; 490 7(5):392-401.
65. Verburg N., Koopman T., Xyaqub M. M., Hoekstra O. S., Lammertsma A. A., Barkhof F., et al. Improved detection of diffuse glioma infiltration with imaging combinations: a diagnostic accuracy study. Neuro Oncol. 2020; 22(3):412-422.
66. Virga, J., Szivos, L., Hortobágyi, T., Chalsaraei, M. K., Zahuczky, G., Steiner, L., et al. (2019). Extracellular matrix differences in glioblastoma patients with different prognoses. Oncol. Lett. 17, 797–806.
67. Wakana, S., Jiang, H., Nagae-Poetscher, L. M., van Zijl, P. C. M., and Mori, S. (2004). Fiber tract-based atlas of human white matter anatomy. Radiology 230, 77–87.
68. Watanabe, M., Tanaka, R., and Takeda, N. (1992). Magnetic resonance imaging and histopathology of cerebral gliomas. Neuroradiology 34, 463–469.
69. Winterstein M., Münter M. W., Burkholder I., Essig M., Kauczor H. U., Weber M. A. Partially resected gliomas: diagnostic performance of fluid-attenuated inversion 474 recovery MR imaging for detection of progression. Radiology. 2010; 254(3):907-16.
70. Wen P. Y., Macdonald D. R., Reardon D. A., Cloughesy T. F., Sorensen A. G., Galanis A., et al. (2010). Updated Response Assessment Criteria for High-Grade Gliomas: Response Assessment in Neuro-Oncology Working Group. Journal of Clinical Oncology 2010; Volume 28, Number 11.

71. Wick, W., Osswald, M., Wick, A., and Winkler, F. (2018). Treatment of glioblastoma in adults. Ther. Adv. Neurol. Disord. 11:1756286418790452.
72. Wirsching, H. G., Galanis, E., and Weller, M. (2016). Glioblastoma. Handb. Clin. Neurol. 134, 381–397.
73. Woodroffe R. W., Zanaty M., Soni N., Mott S. L., Helland L. C., Pasha A., et al. (2020). Survival after reoperation for recurrent glioblastoma. J Clin Neurosci. 73:118-124.
74. Wykes, V., Zisakis, A., Irimia, M., Ughratdar, I., Sawlani, V., and Watts, C. (2021). Importance and Evidence of Extent of Resection in Glioblastoma. J. Neurol. Surg. 82, 75–86.
75. Yamada, K., Sakai, K., Akazawa, K., Yuen, S., and Nishimura, T. (2009). MR tractography: A review of its clinical applications. Magn. Reson. Med. Sci. 8, 165–174.
76. Yan, H., Parsons, D. W., Jin, G., McLendon, R., Rasheed, B. A., Yuan, W., et al. (2009). IDH1 and IDH2 mutations in gliomas. N. Engl. J. Med. 360, 765–773.
77. Yasargil, M. G. (1994). "Neuropathology," in Microneurosurgery Vol. 3B, (New York, NY: Georg Thieme Verlag), 115–192.
78. Young, G. S. (2007). Advanced MRI of adult brain tumors. Neurol. Clin. 25, 947–973.

Appendix 1

Table 1: Patients clinical data

Patients	Age (years) and Sex	Histology	Localization	Side	Time of Diagnosis	Date of Recurrence	Date of Last Follow-up/Death	PFS (months)	OS (months)
1	26 Male	Glioblastoma	Frontalis	Right	2010.03	2012.08	2014.01	28	46
2	54 Female	Glioblastoma	Frontalis	Left	2010.04	2013.02	2013.03	34	35
3	39 Male	Glioblastoma	Parito-occipitalis	Right	2010.07	2012.05	2014.06	22	47
4	47 Male	Glioblastoma	Frontalis	Left	2010.09	2011.01	2012.05	4	20
5	34 Male	Glioblastoma	Frontalis	Left	2010.12	2011.05	2011.10	6	11
6	53 Male	Glioblastoma	Tempro-paritalis	Left	2011.02	2011.06	2012.02	4	12
7	51 Female	Oligodendroglioma-G3	Paritalis	Left	2011.02	2016.03	2017.02	61	72
8	67 Male	Glioblastoma	Temporalis	Left	2012.02	2012.07	2013.02	5	12
9	29 Male	Oligodendroglioma-G3	Fronto-paritalis	left	2012.05	2016.04	2017.09	47	64
10	67 Female	Oligodendroglioma-G3	Frontalis	Right	2012.06	2015.07	2015.07	37	37
11	52 Male	Glioblastoma	Temporalis	Left	2012.09	2013.02	2014.11	5	26
12	68 Male	Glioblastoma	Temporalis	Left	2013.01	2014.02	2014.09	13	20
13	46 Male	Glioblastoma	Frontalis	Right	2019.11	2020.03	2021.02	4	15
14	77 Female	Glioblastoma	Tempro-paritalis	Left	2019.10	2020.06	2020.08	8	10
15	56 Male	Glioblastoma	Paritalis	Left	2019.11	2020.01	2022.03	2	28
16	68 Male	Oligodendroglioma G3	Frontalis	Left	2020.04	2021.012	2022.02	8	10
17	36 Male	Glioblastoma	Parietalis	Left	2020.10	2021.01	2021.04	3	6
18	46 Female	Glioblastoma	Parietalis	Left	2021.01	2022.01	2022.02	1	2
19	55 Male	Glioblastoma	Tempro-parito-occipitalis	Right	2021.02	2021.04	2021.06	2	4
20	59 Male	Glioblastoma	Frontalis	Left	2021.10	2021.12	2022.02	2	3

*PFS, progression free survival; OS, overall survival.

*Patient (1-16): included in FLAIR study, Patient (1-20): included in Tractography study.

Appendix 2

Table 2: The sensitivity and specificity values are listed in this table at each threshold level of the three example cases.

	1%	5%	10%	15%	20%	25%	30%	40%	50%	60%	70%	80%	90%
A													
Sensitivity	0,94	0,80	0,77	0,74	0,66	0,63	0,57	0,46	0,23	0,20	0,14	0,11	0,09
Specificity	0,85	0,96	0,98	0,99	1,00	1,00	1,00	1,00	1,00	1,00	1,00	1,00	1,00
B													
Sensitivity	0,36	0,27	0,23	0,23	0,23	0,23	0,18	0,18	0,09	0,09	0,09	0,05	0
Specificity	0,79	0,85	0,89	0,90	0,90	0,90	0,91	0,91	0,92	0,94	0,96	0,99	0,99
C													
Sensitivity	0,44	0,25	0,25	0,19	0,19	0,19	0,19	0,19	0,19	0,19	0,13	0,13	0
Specificity	1	1	1	1	1	1	1	1	1	1	1	1	1

A: The results of Patient 14 are in concordance with the group average sensitivity and specificity values. B: The sensitivity and specificity of Patient 11. Please note that the specificity is high but the sensitivity is low even at 1% threshold level. This is because there is a smaller part of the recurrent tumor at the original site, which is covered by the TCs, therefore the ratio of the false positive results is low. The main part of the recurrence is far away from the original site, and this will result in a high false negative result. C: The results of Patient 13 are summarized in this table. The specificity is 100% at all threshold level while the sensitivity is very low even at 1%. This is due to the extensive local tumor recurrence which overlaps totally with all TCs It also exceeds its borders and affects several other brain regions resulting in a high rate of false negative results.

Appendix 3

Table 3: The group average sensitivity and specificity values (with standard error of the mean) are listed in this table at each threshold level.

	1%	5%	10%	15%	20%	25%	30%	40%	50%	60%	70%	80%	90%
Sensitivity (Age ± SEM)	0,91±0,03	0,81±0,04	0,73±0,04	0,67±0,05	0,61±0,05	0,60±0,05	0,58±0,06	0,50±0,06	0,35±0,05	0,31±0,06	0,21±0,06	0,14±0,05	0,13±0,06
Specificity (Age ± SEM)	0,81±0,03	0,9±0,02	0,93±0,02	0,95±0,01	0,96±0,01	0,96±0,02	0,92±0,05	0,93±0,05	0,98±0,01	0,94±0,05	0,94±0,04	0,94±0,05	0,94±0,04

*As the threshold increases the sensitivity decreases and the specificity increases. The highest values can be seen at 1 and 5% threshold levels.